Description of quasiparticle and satellite properties via cumulant expansions of the retarded one-particle Green's function

Matthew Z. Mayers,[1] Mark S. Hybertsen,[2] and David R. Reichman[1]

[1]*Department of Chemistry, Columbia University, New York, New York 10027, USA*

[2]*Center for Functional Nanomaterials, Brookhaven National Laboratory, Upton, New York 11973-5000, USA*

A cumulant-based GW approximation for the retarded one-particle Green's function is proposed, motivated by an exact relation between the improper Dyson self-energy and the cumulant generating function. Qualitative aspects of this method are explored within a simple one-electron independent phonon model, where it is seen that the method preserves the energy moment of the spectral weight while also reproducing the exact Green's function in the weak-coupling limit. For the three-dimensional electron gas, this method predicts multiple satellites at the bottom of the band, albeit with inaccurate peak spacing. However, its quasiparticle properties and correlation energies are more accurate than both previous cumulant methods and standard G_0W_0. Our results point to features that may be exploited within the framework of cumulant-based methods and suggest promising directions for future exploration and improvements of cumulant-based GW approaches.

I. INTRODUCTION

The development of methods that can accurately and affordably describe both the total electronic energy and the electronic excitations of complex systems remains a long-standing challenge in both condensed matter physics and chemistry. Substantial progress has been made in recent decades on the development of approximate approaches to calculate correlation contributions that go beyond the Hartree-Fock level of mean-field theory. While density functional theory (DFT), including its extensions to hybrid functionals, has emerged as an accurate and efficient means of calculating many properties of both solids and molecules, systematic improvement of DFT is challenging [1]. In particular, while the Kohn-Sham eigenvalues in the theory often give a surprisingly useful band structure, there are fundamental differences with respect to properly calculated excitation energies [1,2]. More broadly, considering the proliferation of a myriad of approximate exchange-correlation functionals, care must be taken in applications to assess empirical evidence of the accuracy for specific classes of materials.

Separate from DFT, direct many-body methods based on wave functions have achieved impressive accuracy, exemplified by coupled-cluster methods for finite systems [3] and quantum Monte Carlo (QMC) methods for extended systems [4]. These approaches are very challenging numerically due to unfavorable scaling with system size (or complexity), but are often regarded as a "gold standard" when they can be applied. They are also typically more difficult to apply to excited state properties with the same accuracy. Nonetheless, recent progress is encouraging for more widespread application to solids [5–7].

On the other hand, Green's function–based perturbation expansions by their very nature describe spectral features and quasiparticle properties of extended systems in a size-consistent manner [8]. In particular, the development of the GW approximation for application to the one-particle Green's function [9] led to the first predictive calculations of charged excitation energies in real materials [10–13]. The extension to the Bethe-Salpeter equation for the two-particle Green's function has correspondingly supported calculation of the neutral excitations, such as those probed in optical absorption [2]. The development of systematic corrections beyond GW, including approximations to the vertex corrections and the use of self-consistency, remains a subject of ongoing research [14–21]. Interestingly, the corresponding Green's function–based method for the total electronic energy has not been widely used, although several formulations have been investigated [16,22,23].

The homogeneous electron gas model in three dimensions (3D), capturing essential features of the electronic structure of simple metals, has been widely used as a model system. Results based on G_0W_0 (the non-self-consistent first iteration of the GW approximation) show very reasonable quasiparticle properties, but a satellite structure ("plasmaron peak") about $1.5\omega_p$ below the quasiparticle peaks (ω_p being the plasma energy) [24]. This is a surprising result since standard coupled electron-boson models would suggest a series of satellite peaks near integer multiples of ω_p [25] below the quasiparticle peaks. Calculations in which G was iterated to self-consistency, conceptually part of Hedin's original framework [9], indicated further unphysical changes in the satellite region [14,15]. Interestingly, self-consistent GW gave reasonable correlation energies, but it was suggested that vertex corrections were needed in addition to restore physical spectral properties [22].

The difficulty of describing satellite structures in the spectral function strongly suggests a cumulant-based approach to approximately include vertex corrections [26]. This idea has been extensively explored with a time-ordered formulation of G [20,27–32], and has been successful in describing the satellite structure in metals and semiconductors [33–37]. The approach restores the expected satellite progression and modifies the quasiparticle properties quantitatively. In part, the exponential form imposed by the cumulant ansatz leads to the inclusion of higher-order exchange-like diagrams that are only accessible in the standard GW formalism by way of vertex corrections. However, these higher-order diagrams do *not* correspond exactly to standard diagrams in the time-ordered Dyson expansion. More generally, the cumulant approach has not yet reached the formal level of

sophistication that is afforded by the standard diagrammatic apparatus that surrounds the Dyson equation. In particular, aspects related to self-consistency, conservation laws, and the one-to-one correspondence of terms within the cumulant expansion to standard Feynman-Dyson diagrammatics require further investigation.

The time-ordered cumulant approach is limited by the serious drawback that it precludes the possibility of positive spectral weight both above and below the chemical potential. Recently, Kas *et al.* showed that the retarded Green's function is a more natural quantity to employ with the cumulant formalism, as it allows for the description of both particles and holes within one spectral weight profile [38]. Compared with standard G_0W_0 [24], the retarded cumulant approach predicts more physical satellite properties, similar energies, but somewhat less accurate wave-vector-dependent occupation numbers for the 3D electron gas. In this work, we take this retarded Green's function perspective as a starting point to investigate and compare cumulant-based GW schemes.

II. METHODOLOGY

The many-body perturbation expansion for the one-particle Green's function can be resummed via the Dyson equation,

$$
G_k(\omega) = G_k^0(\omega) + G_k^0(\omega)\Sigma_k^I(\omega)G_k^0(\omega),
$$
$$
= G_k^0(\omega)\left[1 + \Sigma_k^I(\omega)G_k^0(\omega)\right] \tag{1a}
$$
$$
= \frac{G_k^0(\omega)}{1 - \Sigma_k^*(\omega)G_k^0(\omega)}, \tag{1b}
$$

where $G_k^0(\omega)$ is the noninteracting Green's function, $\Sigma_k^*(\omega)$ is the proper self-energy, and $\Sigma_k^I(\omega)$ is the improper self-energy [8]. In the non-self-consistent GW approximation (henceforth referred to as G_0W_0), $\Sigma_k^*(\omega)$ is truncated at first order, and the random phase approximation (RPA) $W_k(\omega)$ is used in place of the bare Coulomb interaction v_k [8]:

$$
\Sigma_k^*(\omega) = \frac{i}{\hbar}\frac{1}{(2\pi)^4}\int d^3q\,d\omega'\,G_k(\omega)W_{k-q}(\omega - \omega'), \tag{2a}
$$
$$
W_k(\omega) = \frac{v_k}{1 - \Pi_k(\omega)v_k}, \tag{2b}
$$
$$
\Pi_k(\omega) = \frac{i}{\hbar}\frac{1}{(2\pi)^4}\int d^3q\,d\omega'\,G_q(\omega)G_{k+q}(\omega - \omega'). \tag{2c}
$$

The retarded cumulant ansatz is a resummation of Eqs. (1). It can be written as [38]

$$
G_k^R(t,T) = G_k^{0,R}(t,T)e^{C_k^R(t,T)}, \tag{3}
$$

where $C_k(t,T)$ is the time-local cumulant function and the R superscripts denote retarded quantities.

When considered with Eq. (1a), the cumulant ansatz for the retarded one-particle Green's function leads to a simple closed and exact relation between the *improper* Dyson self-energy and the cumulant generating function:

$$
C_k(t,t') = \ln\left(1 + \left[G_k^{R,0}(t,t')\right]^{-1}\iint dt_1 dt_2\right.
$$
$$
\left. \times G_k^{R,0}(t,t_1)\Sigma_k^{R,I}(t_1,t_2)G_k^{R,0}(t_2,t')\right). \tag{4}
$$

For simplicity, the expressions are written for the electron gas model. While it is clear that Eq. (4) trivially reduces to the standard Dyson equation, it should be noted that such a simple direct and exact relationship between the retarded cumulant and improper retarded Dyson self-energy has, to the best of our knowledge, not been noted before. Such a relation is only possible when retarded quantities and the improper as opposed to the proper self-energy are used. This relation implies new cumulant-like approximations distinct from earlier formulations. For example, the lowest order expansion of the logarithm in conjunction with a retarded, improper self-energy calculated using the normal first-order GW diagrams yields

$$
C_k(t,t') = \left[G_k^{R,0}(t,t')\right]^{-1}\iint dt_1 dt_2\,G_k^{R,0}(t,t_1)\Sigma_{GW,k}^{R,I}(t_1,t_2)
$$
$$
\times G_k^{R,0}(t_2,t'). \tag{5}
$$

This equation for the cumulant (henceforth referred to as G_0W_0 with improper retarded cumulant, or G_0W_0 IRC) is superficially nearly identical to the cumulant approach of Kas *et al.* (G_0W_0 proper retarded cumulant, or G_0W_0 PRC) [38], except that the improper self-energy is used in place of the proper self-energy. To calculate the Green's function within one of these two cumulant schemes, then, a proper or improper retarded self-energy is first computed as in the G_0W_0 scheme. Then the self-energy is inserted into the following Fourier-transformed version of Eq. (5) to find the cumulant:

$$
C_k(t) \equiv C_k(t_0, t_0 + t)
$$
$$
= \int d\omega\,\frac{1}{\pi}\frac{|\mathrm{Im}\Sigma_k^R(\omega + \epsilon_k)|}{\omega^2}(e^{-i\omega t} + i\omega t - 1). \tag{6}
$$

Finally, the spectral weight for the Green's function is obtained by taking a Fourier transform of Eq. (3) [38].

Unlike standard G_0W_0 and G_0W_0 PRC, the cumulant approach outlined above no longer sums diagrams in order of the number of interactions, and is thus not perturbative in the interaction coupling. Instead, the first cumulant in Eq. (5) contains diagrams of all orders of the interaction. We emphasize that this fact renders the approach neither more or less accurate than the more standard G_0W_0 and G_0W_0 PRC approximations. Regardless, the simplicity of the cumulant formalism as outlined above does lead to important properties such as positive and normalized spectral weight [38].

III. RESULTS

To gain a first understanding of the implications of the G_0W_0 IRC approximation, we apply it to the study of a system of independent phonons coupled to a single electronic state:

$$
H = \sum_k \omega_k b_k^\dagger b_k + c^\dagger c\left[\epsilon_c + \sum_k \lambda_k(b_k^\dagger + b_k)\right], \tag{7}
$$

where $b_k, b_k^\dagger$ are the annihilation and creation operators for the phonon states, $c, c^\dagger$ are those of the electronic state, and ϵ_c, λ_k are the excited state electronic energy and the phonon coupling, respectively. We utilize an Einstein spectral density, $J(\omega) = g\delta(\omega - \omega_c)$. This is crudely reminiscent of the plasmon spectral density in the 3D electron gas. This model

has been used previously in the analysis of interaction effects for core-holes [39] and to develop models for valence band spectral functions [22].

For this model Hamiltonian in which the interaction propagator W has been replaced by its phonon propagator analog D, the $G_0 D_0$ PRC approach gives the exact result for the spectral weight [25]. In this regard our goal is not to compare with the standard cumulant approach, which will of course in this model yield "better" results, but to gain an intuition for the expected spectral features produced by the IRC method as well as to see which features of the approach are likely to be well described.

The dynamical part of the proper Dyson self-energy within this model is

$$\Sigma^*(\omega) = \frac{i}{2\pi} \int_{-\infty}^{\infty} d\omega' g \omega_c^2 G^0(\omega - \omega'; \epsilon_c) D^0(\omega'; \omega_c)$$

$$= \frac{i}{2\pi} \int_{-\infty}^{\infty} d\omega' g \omega_c^2 \frac{1}{\omega - \omega' - \epsilon_c + i\delta}$$

$$\times \left(\frac{1}{\omega' - \omega_c + i\delta} - \frac{1}{\omega' + \omega_c - i\delta} \right)$$

$$= \frac{g \omega_c^2}{\omega - \omega_c - \epsilon_c + i\delta}, \qquad (8a)$$

$$|\text{Im } \Sigma^*(\omega)| = \pi g \omega_c^2 \delta(\omega - (\omega_c + \epsilon_c)). \qquad (8b)$$

The frequency integration was done by closing the contour in the lower imaginary half plane. The exact and approximate spectral functions are then evaluated as outlined in the previous section; the improper self-energy is described by

$$|\text{Im } \Sigma^I(\omega)| = \pi g(1 + g)\omega_c^2 \delta(\omega - \omega_c(1 + g) - \epsilon_c), \qquad (9)$$

and the exact and approximate results are

$$A_{\text{PRC}}(\omega) = e^{-g} \sum_{l=0}^{\infty} \frac{g^l}{l!} \delta(\omega - \epsilon_c + g\omega_0 - \omega_0 l), \qquad (10)$$

$$A_{G_0 D_0}(\omega) = \frac{1}{1 + g} \delta(\omega - \epsilon_c + g\omega_0)$$

$$+ \frac{g}{1 + g} \delta(\omega - \epsilon_c - \omega_0), \qquad (11)$$

$$A_{\text{IRC}}(\omega) = e^{-g/(1+g)} \sum_{l=0}^{\infty} \frac{1}{l!} \left(\frac{g}{1 + g} \right)^l$$

$$\times \delta(\omega - \epsilon_c + g\omega_0 - \omega_0 l(1 + g)), \qquad (12)$$

respectively. The exact solution describes a sequence of peaks separated by multiples of ω_0 in energy. The basic $G_0 D_0$ (Dyson) approximation predicts just two peaks, a quasiparticle peak and a satellite peak separated by $\omega_0(1 + g)$, while the $G_0 D_0$ IRC formulation predicts an infinite series of peaks separated by $\omega_0(1 + g)$. The $G_0 D_0$ IRC spectrum inherits the unphysical spacing from the $G_0 D_0$ improper self-energy, which becomes correct only in the weak-coupling ($g \ll 1$) limit. It is easy to check that all three methods give normalized

spectral weights with an identical first moment

$$\left\langle \left| \left| cc^\dagger \left(\epsilon_c + \sum_k \lambda_k(b_k^\dagger + b_k) \right) \right| \right| \right\rangle = \int \omega A(\omega) d\omega = \epsilon_c, \quad (13)$$

where $|\rangle$ represents the direct product of the ground electronic state and all ground phonon states. The $G_0 D_0$ IRC spectrum, although inaccurate in its peak spacing, still encodes the correct first energy moment. Thus, the IRC approach appears, within this simple toy model, to embody a compromise between the standard cumulant and self-energy GW approaches. Furthermore, it appears not to corrupt some important aspects of the problem, such as the existence of multiple satellites and the value of the "correlation" energy.

The electron gas problem provides a more stringent and informative grounds of comparison for the different approximation schemes because no known method, including the $G_0 W_0$ PRC scheme, is exact. Although the electron gas Hamiltonian differs significantly from the form of Eq. (7), many of the observations made earlier about the three approximations to the Green's function should still apply. In Figs. 1(a) and 1(c),
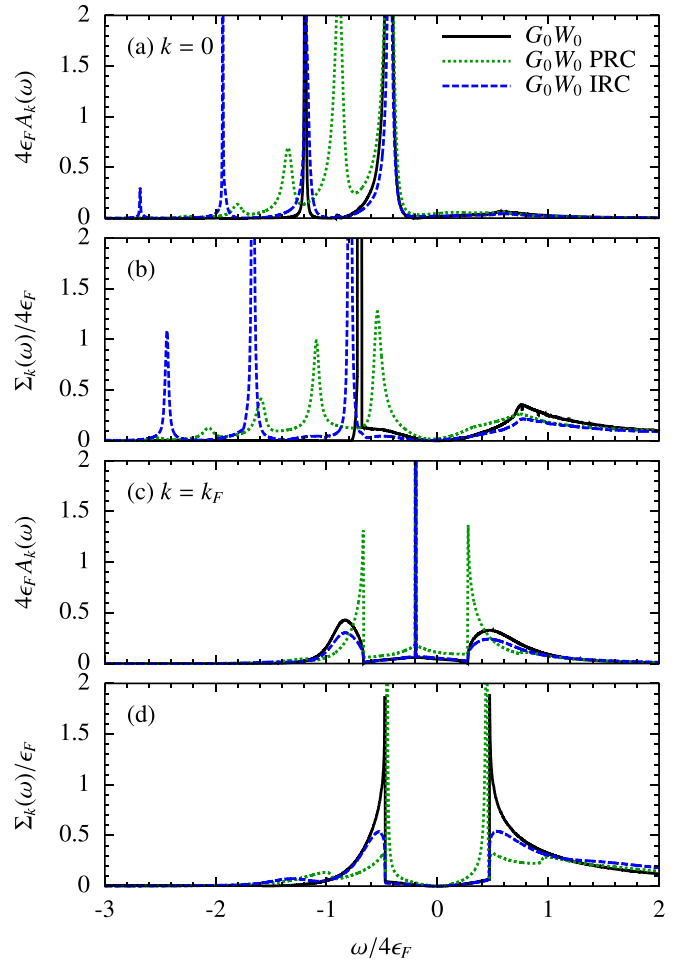

FIG. 1. A comparison of three distinct GW schemes. (a), (c) The spectral weight for the 3D electron gas with $r_s = 4.0$. (b), (d) The absolute value of the imaginary part of the proper self-energy, solved using Dyson's equation, corresponding to the spectral weights in (a) and (c).
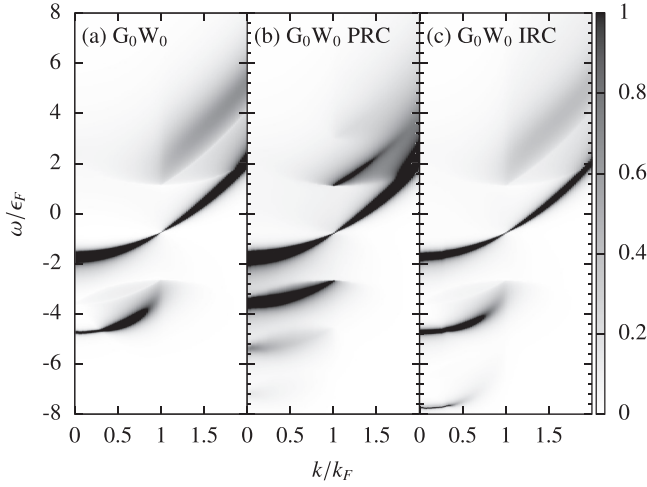
FIG. 2. Band structure for various GW schemes at $r_s = 4$. Note that the G_0W_0 IRC contains multiple satellites, similar to the G_0W_0 PRC case, but with a spacing that mimics the incorrect position of the G_0W_0 plasmaron peak.

we present the spectral weight

$$A_k(\omega) = -\frac{1}{\pi} \text{Im} G_k^R(\omega) \qquad (14)$$

for the 3D electron gas at density $r_s = 4.0$ both at the Fermi energy and at the bottom of the band. The spectral weight for the Dyson GW self-energy is plotted for the same cases in Figs. 1(b) and 1(d). The full band structure is reported for all three calculation schemes in Fig. 2.

Both cumulant schemes improve the qualitative description of the satellite region at low k: whereas the G_0W_0 scheme predicts just one satellite at an energy $1.5\omega_p$ below the quasiparticle (QP) peak, both cumulant schemes predict a series of evenly spaced satellites with decreasing weights. The G_0W_0 PRC scheme predicts that these satellite peaks are separated by approximately the plasmon energy ω_p, whereas the G_0W_0 IRC scheme inherits the (presumably unphysical) $\sim 1.5\omega_p$ spacing from the G_0W_0 calculation, exactly as it did in the electron-phonon model explored earlier. At and above the Fermi wave vector k_F, the G_0W_0 IRC results are much more similar to the G_0W_0 results as compared to those from the G_0W_0 PRC. Overall, the G_0W_0 IRC scheme interpolates between the rounded spectral behavior of G_0W_0 at larger k and the multiple satellite peak behavior of G_0W_0 PRC at lower k.

In addition to the spacing of satellite peaks, another unphysical feature of the IRC approach is the appearance of spurious sharp quasiparticle resonances which are most apparent in the unoccupied portion of the spectral function. These features can be easily removed in a manner that hardly affects $A_k(\omega)$ for $k \leqslant k_F$, $n(k)$, or ϵ_{corr}/N (the latter two of which are discussed next). The origin of these features and the means for their removal are discussed in the Appendix.

While the results for the 3D electron gas in the high-frequency satellite wing suggest that the G_0W_0 PRC is most accurate in this spectral region, these results shed little light on other properties, to which we now turn. We present in Fig. 3
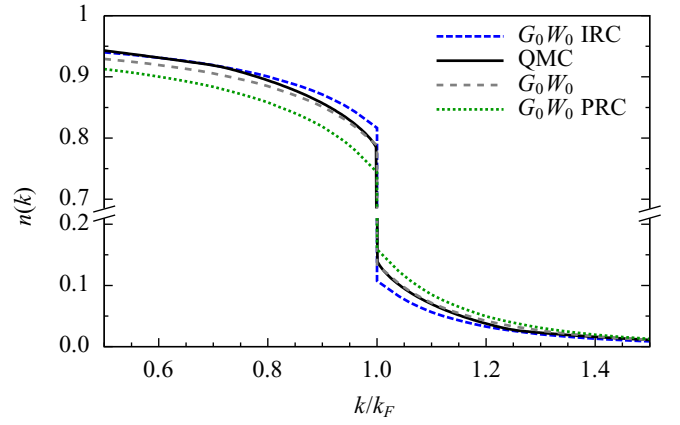

FIG. 3. The k-dependent occupation number $n(k)$ for all three approximation schemes at $r_s = 4.0$, plotted against the "exact" QMC result [40,41].

the wave-vector-dependent occupation number

$$n_k = \int_{-\infty}^{\mu} A_k(\omega) d\omega. \qquad (15)$$

The G_0W_0 IRC scheme performs similarly to G_0W_0, erring on the opposite side of the "exact" quantum Monte Carlo (QMC) data [40,41]. Notably, the G_0W_0 IRC occupation numbers match the QMC results almost exactly for $k < 0.9k_F$ and $k > 1.1k_F$; although the scheme suffers from unphysical satellite peak spacing at small k, it inherits rather accurate occupation numbers from G_0W_0. The G_0W_0 PRC occupation numbers are not as accurate, and yield a QP renormalization factor which is too small.

The accuracy of the occupation numbers in the G_0W_0 IRC approximation can be explained using the self-energy spectra in Figs. 1(b) and 1(d). The most significant dependence of the momenta are on the weight of the main QP peak, which is determined by the slope of the real part of the self-energy. Since the real and imaginary parts of the self-energy are related by a Kramers-Kronig transform, the slope of the real part of the self-energy depends most strongly on the weight and positions of the peaks in the self-energy spectrum closest to $\omega \simeq \epsilon_k$. Since the G_0W_0 IRC self-energy spectrum peaks are more similar to the G_0W_0 ones, one would expect the G_0W_0 IRC momentum distribution near $k = k_F$ to more closely resemble that of G_0W_0. In particular, the increased QP renormalization factor with respect to the G_0W_0 approximation is explained

TABLE I. Correlation energies of the 3D electron gas per particle ϵ_{corr}/N in hartrees for various GW schemes and r_s values [42]. QMC values are obtained from Vosco *et al.*'s parametrization [43] of Ceperley and Alder's fixed-node diffusion Monte Carlo data [44].

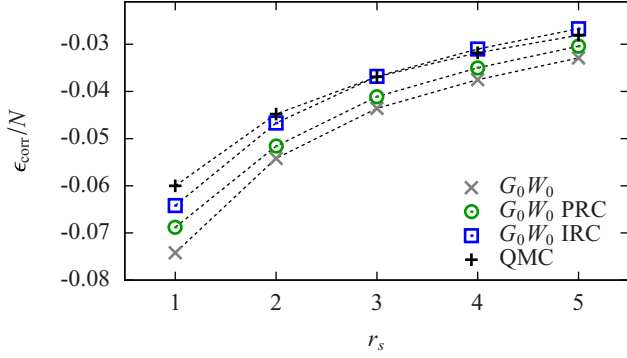| r_s	G_0W_0	G_0W_0 PRC	G_0W_0 IRC	QMC
1	−0.0742	−0.0688	−0.0642	−0.0600
2	−0.0542	−0.0516	−0.0467	−0.0448
3	−0.0436	−0.0411	−0.0368	−0.0369
4	−0.0375	−0.0350	−0.0310	−0.0318
5	−0.0329	−0.0304	−0.0267	−0.0281

FIG. 4. Correlation energies of the 3D electron gas per particle ϵ_{corr}/N for various GW schemes and r_s values compared with the "exact" QMC result. Exact values are reported in Table I.

by the slightly smaller peaks in the G_0W_0 IRC self-energy spectrum at $k = k_F$.

Finally, total energies may be calculated from $A_k(\omega)$ using the Galitskii-Migdal formula

$$\epsilon = \sum_k \int_{-\infty}^{\mu} (\omega + \epsilon_k) A_k(\omega) d\omega, \quad (16)$$

where $\epsilon_k = k^2/2$ is the free-electron energy dispersion. The correlation energy per particle is calculated using $\epsilon_{\text{corr}} = (\epsilon - \epsilon_{\text{HF}})/N$, where ϵ_{HF} is the Hartree-Fock energy. For the cumulant schemes, μ is determined by enforcing the total particle number. These energies are reported in Table I and plotted in Fig. 4. For reference, the results from fixed-node diffusion Monte Carlo calculations of Ceperley and Alder [44] are shown based on the parametrization by Vosko and coworkers [43]. The G_0W_0 IRC scheme yields significantly more accurate correlation energies as compared to earlier schemes over this important range of r_s values.

IV. CONCLUSION

In this work, we motivate the use of the improper retarded self-energy in the cumulant generating function using Dyson's equation. Non-self-consistent calculations of the spectral weight show that the improper retarded cumulant (IRC) scheme predicts a series of multiple satellite bands with a larger-than-expected spacing at the bottom of the band. However, compared to the G_0W_0 PRC scheme, which predicts a series of satellite bands with a more physical ω_p spacing, the IRC scheme yields noticeably improved occupation numbers and correlation energies. This is promising in the ongoing research directed to unified, efficient approaches for both total electronic energy and excitation energies. Further work should be done to investigate other aspects related to the retarded cumulant-based GW approaches discussed here, including self-consistency and the influence of higher-order cumulants.

Note added. Recently, several related studies have appeared [45–47]. The spectral weights reported in these works for the electron gas model in the G_0W_0 PRC approximation are identical to the ones presented here.

APPENDIX : SPURIOUS SHARP QUASIPARTICLE RESONANCES AT $k > k_F$

The standard description of the cumulant function requires the evaluation of

$$C_k(t) = \frac{1}{\pi} \int d\omega \frac{|\text{Im}\Sigma(\omega + \epsilon_k)|}{\omega^2} (e^{-i\omega t} + i\omega t - 1), \quad (A1)$$

which for the IRC demands that the integrand be constructed with $\text{Im}\Sigma^{I,R}(\omega + \epsilon_k)$. It should be noted, however, that the geometric sequence that is the improper self-energy is ill-defined when evaluated precisely on the energy shell since $G_k^0(\epsilon_k)$ is divergent there. This divergence implies $\text{Im}\Sigma^{I,R}(\epsilon_k) = 0$, resulting in a sharp quasiparticle-like feature in $A_k(\omega)$ superimposed on a smooth continuum. This feature is most apparent for $k > k_F$, as can be seen in Fig. 5(a). Note that the smooth continuum behavior is much like that of the standard G_0W_0 spectral function.

This feature may be removed in a variety of ways that preserve all of the conclusions reached in the main text. For example, if the cumulant function $C_k(t)$ is defined such that the evaluation of $\text{Im}\Sigma_k(\omega + \epsilon_k^{G_0W_0})$ is used as opposed to $\text{Im}\Sigma_k(\omega + \epsilon_k)$, then no spurious resonance appears (rIRC). In addition, $A_k(\omega)$ for $k \leqslant k_F$, $n(k)$, and ϵ_{corr}/N are essentially unchanged. The same outcome occurs if the frequency of
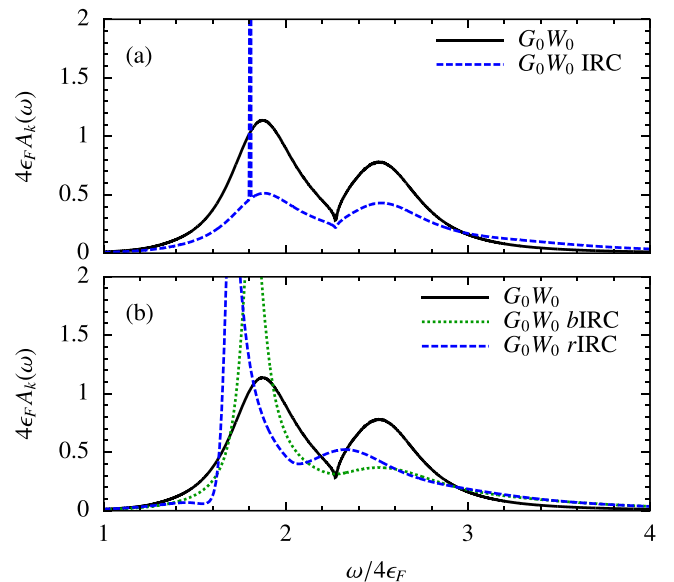

FIG. 5. Band structure for various GW schemes at $r_s = 4$ and $k = 3k_F$. The sharp quasiparticle resonance predicted by G_0W_0 IRC is broadened by the bIRC and rIRC schemes.

$G_k^0(\omega)$ within $\Sigma_k^{I,R}(\omega)$ is given an imaginary part equal to $\Sigma_k^*(\epsilon_k^{G_0 W_0})$, the quasiparticle lifetime associated with a standard $G_0 W_0$ calculation (bIRC).

These distinct regularization procedures do however alter the shape of $A_k(\omega)$ for $k > k_F$ as shown in Fig. 5(b). Table II shows the robustness of the correlation energies for the different schemes; we do not replot $A_k(\omega)$ for $k \leqslant k_F$ or $n(k)$ because they are essentially unaltered from Figs. 1, 2, and 3. Overall, we find that the most important features of the IRC approach are basically unmodified under the removal of these spurious resonances.

TABLE II. Correlation energies of the 3D electron gas per particle $\epsilon_{\mathrm{corr}}/N$ in hartrees for the broadened IRC (bIRC) and the renormalized IRC (rIRC) schemes.

r_s	$G_0 W_0$ IRC	$G_0 W_0$ bIRC	$G_0 W_0$ rIRC	QMC
1	-0.0642	-0.0643		-0.0600
2	-0.0467	-0.0467		-0.0448
3	-0.0368	-0.0363		-0.0369
4	-0.0310	-0.0304	-0.0308	-0.0318
5	-0.0267	-0.0260		-0.0281

[1] A. J. Cohen, P. Mori-Sánchez, and W. Yang, Chem. Rev. **112**, 289 (2012).

[2] G. Onida, L. Reining, and A. Rubio, Mod. Rev. Phys. **74**, 601 (2002).

[3] R. J. Bartlett and M. Musiał, Rev. Mod. Phys. **79**, 291 (2007).

[4] W. M. C. Foulkes, L. Mitas, R. J. Needs, and G. Rajagopal, Rev. Mod. Phys. **73**, 33 (2001).

[5] G. H. Booth, A. Gruneis, G. Kresse, and A. Alavi, Nature (London) **493**, 365 (2013).

[6] J. J. Shepherd and A. Grüneis, Phys. Rev. Lett. **110**, 226401 (2013).

[7] J. McClain, J. Lischner, T. Watson, D. A. Matthews, E. Ronca, S. G. Louie, T. C. Berkelbach, and G. K.-L. Chan, Phys. Rev. B **93**, 235139 (2016).

[8] L. Hedin and S. Lundquist, in *Solid State Physics*, edited by F. Seitz and D. Turnbull (Academic, New York, 1969), p. 1.

[9] L. Hedin, Phys. Rev. **139**, A796 (1965).

[10] M. S. Hybertsen and S. G. Louie, Phys. Rev. B **34**, 5390 (1986).

[11] R. W. Godby, M. Schlüter, and L. J. Sham, Phys. Rev. B **35**, 4170 (1987).

[12] F. Aryasetiawan and O. Gunnarsson, Rep. Prog. Phys. **61**, 237 (1998).

[13] W. G. Aulbur, L. Jönsson, and J. W. Wilkins, in *Solid State Physics* (Academic, New York, 2000), p. 1.

[14] E. L. Shirley, Phys. Rev. B **54**, 7758 (1996).

[15] U. von Barth and B. Holm, Phys. Rev. B **54**, 8411 (1996).

[16] B. Holm and U. von Barth, Phys. Rev. B **57**, 2108 (1998).

[17] F. Bruneval, F. Sottile, V. Olevano, R. Del Sole, and L. Reining, Phys. Rev. Lett. **94**, 186402 (2005).

[18] M. van Schilfgaarde, T. Kotani, and S. Faleev, Phys. Rev. Lett. **96**, 226402 (2006).

[19] M. Shishkin, M. Marsman, and G. Kresse, Phys. Rev. Lett. **99**, 246403 (2007).

[20] M. Guzzo, G. Lani, F. Sottile, P. Romaniello, M. Gatti, J. J. Kas, J. J. Rehr, M. G. Silly, F. Sirotti, and L. Reining, Phys. Rev. Lett. **107**, 166401 (2011).

[21] A. Grüneis, G. Kresse, Y. Hinuma, and F. Oba, Phys. Rev. Lett. **112**, 096401 (2014).

[22] B. Holm and F. Aryasetiawan, Phys. Rev. B **62**, 4858 (2000).

[23] N. E. Dahlen, R. van Leeuwen, and U. von Barth, Phys. Rev. A **73**, 012511 (2006).

[24] B. I. Lundqvist, Phys. Kondens. Materie **7**, 117 (1968).

[25] G. D. Mahan, *Many-Particle Physics*, 3rd ed. (Kluwer Academic/Plenum Publishers, New York, 2000).

[26] R. Kubo, J. Phys. Soc. Jpn. **17**, 1100 (1962).

[27] L. Hedin, Phys. Scr. **21**, 477 (1980).

[28] C.-O. Almbladh and L. Hedin, *Beyond the One-Electron Model: Many-Body Effects in Atoms, Molecules, and Solids* (North-Holland, New York, 1983), pp. 607–904.

[29] F. Aryasetiawan, L. Hedin, and K. Karlsson, Phys. Rev. Lett. **77**, 2268 (1996).

[30] B. Holm and F. Aryasetiawan, Phys. Rev. B **56**, 12825 (1997).

[31] M. Vos, A. S. Kheifets, V. A. Sashin, E. Weigold, M. Usuda, and F. Aryasetiawan, Phys. Rev. B **66**, 155414 (2002).

[32] J. Lischner, D. Vigil-Fowler, and S. G. Louie, Phys. Rev. B **89**, 125430 (2014).

[33] J. Lischner, D. Vigil-Fowler, and S. G. Louie, Phys. Rev. Lett. **110**, 146801 (2013).

[34] M. Guzzo, J. J. Kas, L. Sponza, C. Giorgetti, F. Sottile, D. Pierucci, M. G. Silly, F. Sirotti, J. J. Rehr, and L. Reining, Phys. Rev. B **89**, 085425 (2014).

[35] F. Caruso, H. Lambert, and F. Giustino, Phys. Rev. Lett. **114**, 146404 (2015).

[36] F. Caruso and F. Giustino, Phys. Rev. B **92**, 045123 (2015).

[37] J. S. Zhou, J. J. Kas, L. Sponza, I. Reshetnyak, M. Guzzo, C. Giorgetti, M. Gattie, F. Sottile, J. J. Rehr, and L. Reining, J. Chem. Phys. **143**, 184109 (2015).

[38] J. J. Kas, J. J. Rehr, and L. Reining, Phys. Rev. B **90**, 085112 (2014).

[39] D. C. Langreth, Phys. Rev. B **1**, 471 (1970).

[40] M. Holzmann, B. Bernu, C. Pierleoni, J. McMinis, D. M. Ceperley, V. Olevano, and L. Delle Site, Phys. Rev. Lett. **107**, 110402 (2011).

[41] V. Olevano, A. Titov, M. Ladisa, K. Hämäläinen, S. Huotari, and M. Holzmann, Phys. Rev. B **86**, 195123 (2012).

[42] Slight differences in the PRC energies from those presented in Ref. [38] are due to differing underlying GW self-energies. These differences are on the order of the numerical uncertainty in the correlation energy as calculated using Eq. (16) .

[43] S. H. Vosko, L. Wilk, and M. Nusair, Can. J. Phys. **58**, 1200 (1980).

[44] D. M. Ceperley and B. J. Alder, Phys. Rev. Lett. **45**, 566 (1980).

[45] B. Gumhalter, V. Kovač, F. Caruso, H. Lambert, and F. Giustino, Phys. Rev. B **94**, 035103 (2016).

[46] F. Caruso and F. Giustino, arXiv:1606.08573.

[47] D. Vigil-Fower, S. G. Louie, and J. Lischner, Phys. Rev. B **93**, 235446 (2016).